Near-field Circular Array for the Transcutaneous Telemetry of UHF RFID-based Implantable Medical Devices

C. Miozzi, *Student Member, IEEE*, G. Saggio, E. Gruppioni, and G. Marrocco, *Member, IEEE*

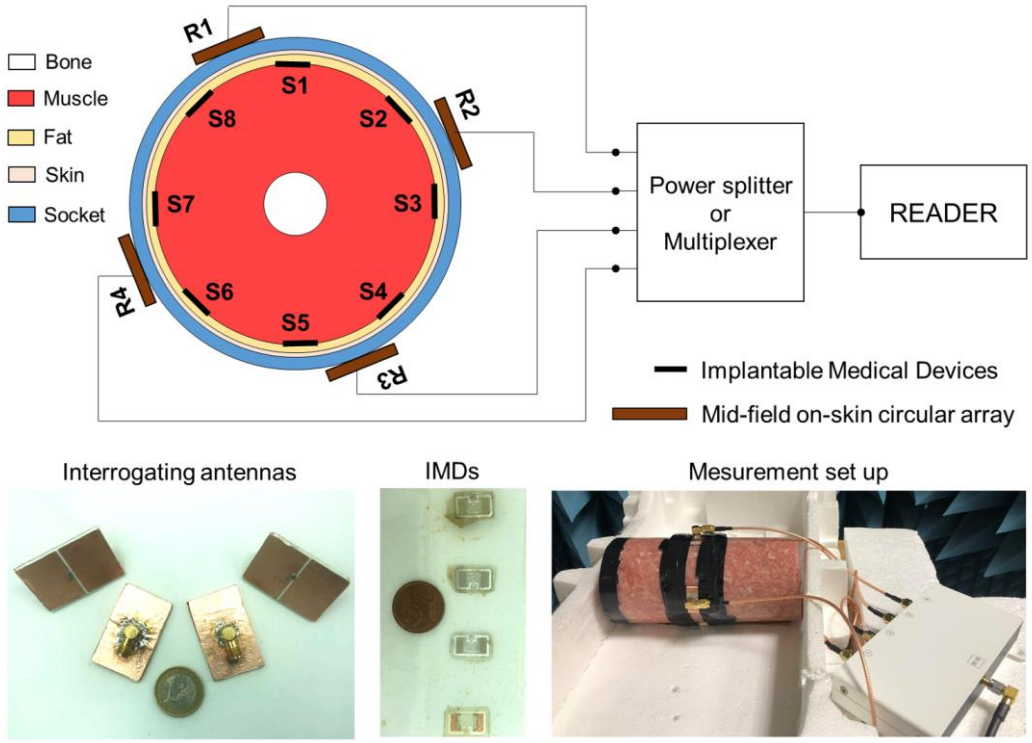

Visual Summary: Scheme of the circular array interrogator, composed by four on-skin antennas fed by a power splitter or a multiplexer, and of the eight IMDs in a simplified human arm model (top). Interrogating and implanted antenna prototypes and realistic mock-up of measurement (bottom).

Take-Home Messages

- This work exploits the potentiality of a circular array of interrogating antennas to establish a robust RFID-based transcutaneous link with multiple Implantable Medical Devices with no battery onboard and also accounting for the safety constraints.
- Thanks to the use of the array configuration, the minimum SAR-compliant power required to energize up to eight IMDs hosting the state-of-the-art sensor-oriented ICs, is less than 23 dBm, well compatible with portable small RFID readers.
- The capability to monitor multiple IMDs over a large region of the human body is particularly useful in some biomedical applications, such as the control of prosthetic hand through Electromyographic sensors, with increased degrees of freedom in driving actuators.
- The radiative near-field circular array permits to establish a robust transcutaneous telemetry with multiple IMDs, thus enlarging the read region inside the human body for multi-point monitoring of physiological parameters, with a robust power margin and in compliance with the electromagnetic exposure regulations.
- The transcutaneous telemetry of a multi-antenna array with multiple implanted sensors was studied, both numerically and experimentally, considering a circularly body region (*i.e.* limbs), but the findings of this work go far beyond this example of application with innovative and promising advancements in the whole realm of Implantable Medical Devices.

Near-field Circular Array for the Transcutaneous Telemetry of UHF RFID-based Implantable Medical Devices

C. Miozzi, *Student Member*, *IEEE*, G. Saggio, E. Gruppioni, and G. Marrocco, *Member*, *IEEE*

***Abstract*—Wireless communication with Implantable Medical Devices (IMDs) based on Radiofrequency Identification in the UHF band suffers from the constraints on the maximum power absorbed by the body tissues. Accordingly, an interrogating antenna placed onto the skin is capable to monitor only a limited region just below its footprint. In some applications like the hand prosthesis controlled by Electromyographic signals emitted by muscle contractions, multiple IMDs have to be used to increase the degrees of freedom in driving the actuators. An array of interrogators, working in the near-field can mitigate this bottleneck by greatly extend the read region inside the body. Sequentially- and simultaneously-fed arrays by a same reader are here investigated to optimize the multi-sensor backscattering modulated links. The conditions (feeding scheme and alignment) to guarantee a robust interrogation of a relevant number of implanted sensors with no battery onboard are identified also accounting for the safety constraints related to the SAR. Numerical simulations and experimentation with a cylindrical phantom resembling human limbs, hosting reference antennas, demonstrate that the simultaneous feed permits to interact with eight IMDs by using nearly all the available power from typical readers (30 dBm, 22 dBm as a minimum) without exceeding the SAR limit with a power margin (w.r.t. sensor-oriented ICs with -10 dBm power sensitivity) of more than 5 dB for any angular alignment between the array and the sensors.**

***Index Terms*—Implantable Medical Devices, Radiofrequency Identification, Transcutaneous Telemetry, Wireless Power Transfer.**

I. Introduction[1]

Implantable Medical Devices (IMDs) can wirelessly monitor the health of prosthesis and, more in general, the patient physiological data in real-time [1], [2] from the inside. They are currently applied in clinical practice as integrated into cardiac pacemakers and defibrillators. Further emerging applications concern visual prosthesis [3], brain-computer interfaces [4], [5], embedded monitoring of oxygen [6], glucose [7], [8], pH level [9], intracranial pressure [10], rise of local temperature following inflammations [11] and of electrical biosignals [12]. The size and durability of IMDs are fundamental requirements [13]. The highest simplification of the electronic complexity can be achieved by resorting to the Radiofrequency Identification (RFID) technology [11], [14], [15], [16], so that the implantable sensor can be reduced to an antenna for energy harvesting, an IC (Integrated Circuit) transponder and a dedicated sensor. The battery can be in principle avoided by exploiting the passive communication with an external reader through the backscattering modulation of the IMD load [17]. Flexible and conformable layouts of IMDs have been already investigated [18].

Recently, the authors demonstrated [19], [20] the feasibility of an RFID-based transcutaneous wireless communication through the arm in the UHF band (860-960 MHz) to capture the myoelectric signals generated by muscular contractions to control hand prostheses for amputees. In particular, the actuators can be controlled by the electric signals produced by the contraction of the residual muscles in the stump of the amputated hand. Preliminary experiments involved a single interrogating antenna, namely a microstrip slot placed on the skin, and small loops as implanted antennas [19]. Moreover, the authors verified the possibility to detect Electromyographic (EMG) signals by using a really simplified and minimized radio-circuitry for data transmission, just based on the AMS-SL900A chipset [20]. The averaged reading rate was 28 Hz which, even though much lower than the 1 kHz sampling rate provided by state-of-the-art equipment [21], was nevertheless enough to correctly identify the muscle contractions and to estimate their duration thus providing the user with control over a single degree of freedom, such as hand opening/closing. Higher sampling rate (from 60 Hz up to 1 kHz) have been obtained as well through RFID-based platforms [22], [23], at the cost of a more complex circuitry. A higher degree of freedom in the prosthesis control could be achieved by using multiple implanted sensors to monitor the activity of groups of flexor and extensor muscles [24].

The bottleneck of transcutaneous link based on RFID [25] is generally related to the compliance with the electromagnetic exposure regulations, in terms of the Specific Absorption Rate - (SAR). Indeed, the very low efficiency of an implanted antenna and the modest sensitivity of RFID ICs implementing backscattering-based protocols, demand for a high transmitted power that in turn generates a risky exposure condition for the body. Simulations and experimentations revealed that the maximum power that can be continuously emitted by an on-skin reader [26], in compliance with the safety constraints (SAR averaged on 10 g less than 4 W/kg in the limbs), must be less than 23 dBm in the worst case of continuous illumination and neglecting the duty-cycle of the RFID protocol. In consequence, establishing a telemetry link with the deepest implanted battery-less sensors is a challenging task. In the state-of-the-art, the transcutaneous link can be correctly

[1]C. Miozzi and G. Saggio are with the Department of Electronic Engineering, University of Roma Tor Vergata, 00133 Rome, Italy. E. Gruppioni is with INAIL Centro Protesi, Research and Training Area, 40054 Budrio, Italy. G. Marrocco is with the Department of Civil Engineering and Informatics, University of Roma Tor Vergata, 00133 Rome, Italy. Corresponding author: Gaetano Marrocco, gaetano.marrocco@uniroma2.it.

activated with the only device that is implanted just beneath the interrogator. Multiple implanted sensors will then require a more advanced interrogation architecture.

In this paper, a multi-antenna interrogation system is proposed, with the purpose to increase the number of RFID IMDs that can be read with a robust power margin. The paper is in particular focused on IMDs inside cylindrical-like regions, resembling limbs.

Wearable multi-antenna systems have been already proposed for the localization of endoscopic capsules by using radio frequency-based methods [27], [28], [29], [30]. They are mostly used in receiving modes to collect the signals emitted by active IMDs working in transmitting mode. The instantaneous position of the moving IMD can be hence estimated by processing the received-signal strength (RSS), the time-of-arrival (TOA), or the angle-of-arrival (AOA). Transmitting arrays of on-body antennas, driven in coherent or incoherent modes, are instead widely used in microwave hyperthermia. However, these arrangements were not used for transcutaneous communication as their only aim is to enforce on the SAR deposition pattern [31], [32], [33] maximizing the energy delivery to localized targets, while preserving the healthy organs.

In this paper, the concept of RFID array is instead investigated for the first time concerning the communication with IMDs working according to the modulated backscattering. The purpose is achieving a spatial field homogeneity in large region of the limb so that a robust link with a multiplicity of IMDs can be established. The described analysis will determine the conditions (feeding scheme and alignment) to guarantee the robust interrogation of a relevant number of implanted sensors with no battery onboard, also accounting for the safety constraints related to the SAR. Two different types of power supply (sequential and simultaneous feeding) are considered and the performance are parameterized in terms of the SAR-compliant power margin (Section II). The idea is hence exploited, by numerical simulations for the case of devices suitable for implantation into the arm, for instance for the monitoring of the myoelectric signals (Section III). Finally, prototypes of all the components are used to experimentally evaluate the transcutaneous links (Section IV) and corroborate the numerically predicted power margins.

II. Array Arrangements and Parameterization

The multi-antenna transcutaneous telemetry system (Fig. 2) comprises *M* interrogating external antennas, forming an equally-spaced circular array, which is placed around the body region to be monitored or even on its surface. Without any loss of generality, the implanted sensors are arranged along an *N*-elements circular array, co-planar with the previous one, that is placed inside the body.

Two types of feeding (Fig. 1a-b) are considered: *sequential* and *simultaneous*.

A. Sequential feeding

In the sequential feeding scheme (Fig. 1a), the interrogating antennas are sequentially powered by the generator through a multiplexer having insertion loss L_M so that only an antenna is instantaneously active. IMDs will be therefore read at different times. Denoting with P_G the total available power of the generator, the *m*th antenna will be then sourced by $P_{G,m} = P_G/L_M$.

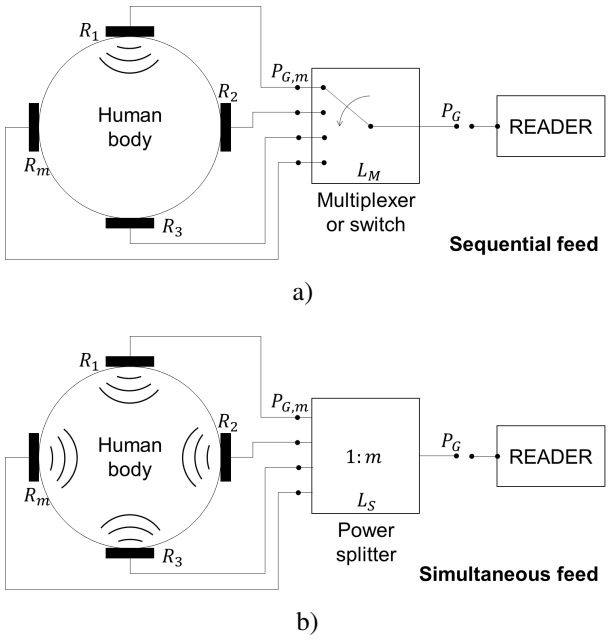

Figure 1. Feeding schemes of the interrogating array for a) sequential and b) simultaneous interrogations.

The efficiency in the power transfer is quantified by the *embedded transducer power gain* [11] $G_{T,n(m)}$, defined as the ratio between the power $P_{n(m)}$ delivered to the nth IMD by the mth transmitting antenna, when the remaining $M-1$ are switched-off (open-circuit termination), and the total available power of the generator:

$$G_{T,n(m)} = \frac{P_{n(m)}}{P_G} = \frac{P_{n(m)}}{P_{G,m} L_M}. \quad (1)$$

This indicator also accounts for possible impedance mismatch at both reader and IMD sides as well as it includes the electromagnetic coupling among transmitters and receivers in the radiating near-field region where both electric and magnetic phenomena are involved [34].

Referring to a typical COTS MUX [35], the size without enclosure is $72 \times 92 \times 17$ mm^3. This is a general-purpose device, and a further miniaturization can be feasible with an ad-hoc optimized design. The declared current consumption is < 12 mA that is negligible w.r.t. that of a typical wearable RFID reader (~570 mAh [36]). The required power can be then provided by the same battery sourcing of the reader with no expected sensible reduction of the system autonomy.

B. Simultaneous feeding

In the simultaneous feeding scheme (Fig. 1b), the interrogating antennas are always connected to the power source through a power splitter having insertion loss L_S. In this case, each interrogating antenna will be fed by $P_{G,m} = \frac{P_G}{M L_S}$ and

all IMDs will be interrogated simultaneously. The resulting array is therefore coherent so that the total radiated field inside the body is the vectorial superposition of the fields produced by each interrogating antenna in presence of the others being disconnected from the sources. The SAR will be hence derived from the square value of the before-mentioned total field.

The performance parameter is the *active transducer power gain* $G_{T,n}$, namely the ratio between the power P_n delivered to the nth IMD when all the interrogators are switched on, according to the scheme in Fig. 1b, and the total available power from the generator:

$$G_{T,n} = \frac{P_n}{P_G} = \frac{P_n}{ML_S P_{G,m}}. \quad (2)$$

C. Link Margin

By assuming, for simplicity, that IMDs include IC transponders of a same family, with power sensitivity p_{IC}, the minimum power required by the reader to activate the *n*th implanted sensor, so that[2] $P_n = p_{IC}$, is :

$$P_{G,n}^{min} = \frac{p_{IC}}{G_{T,n}}. \quad (3)$$

Let $P_G^{max}(SAR_0)$ be the maximum power continuously emitted by the reader so that the corresponding SAR delivered in the body is less than the regulation limit SAR_0, the feasibility of the link can be quantified by the *constrained power margin* referred to the turn-on of the *n*th IMD:

$$M_n = \frac{P_G^{max}(SAR_0)}{P_{G,n}^{min}}. \quad (4)$$

The *n*th IMD is then activated by the reader, provided that $M_n > 1$. M_n hence gives a measure of the power in excess, w.r.t. the available one, in the communication between the interrogating system and the generic implanted device. The parameter M_n quantifies the reliability of the link with the *n*th IMD. From (3) the margin can be expressed in terms of the transducer power gain as:

$$M_n = \frac{P_G^{max}(SAR_0)}{\alpha p_{IC}} G_{T,n} \quad (5)$$

where $\alpha > 1$ is an additional safeguard margin, hereafter fixed to 2 (3 dB) accounting for non-fully predictable parameters of the system.

III. Numerical analysis: loops in the arm and on-skin slot interrogators

Without loss of generality, let consider the case of $M = 4$ interrogators and $N = 8$ IMDs placed at the muscle-fat interface of an arm. This arrangement can be useful for the detailed monitoring of the electromyographic signals on the agonist and antagonist muscles [26] of the forearm of an amputee for hand prosthesis control.

[2]the notation P_n and $G_{T,n}$ will be hereafter used for both simultaneous and sequential feedings. For the latter case, the "*n*" subscript must be read as $n(m)$.

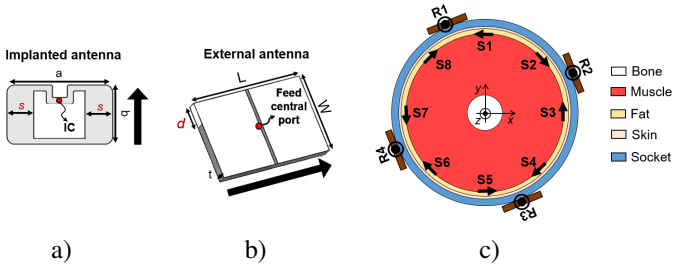

a) b) c)

Figure 2. Reference antennas for the transcutaneous telemetry system: a) the loop implanted transponder and b) the interrogating microstrip slot. Relevant size (in [mm]): $a = 13$, $b = 8$, $s = 2.5$, $L = 40$, $W = 25$, $t = 3$, $d = 1$. Arrows indicate the reference directions to identify the placement in the body. c) Cross-section view of the simplified arm model with the circular array interrogator, composed by four microstrip slots, and eight implanted loops. Black circles indicate outgoing arrows, thus according to the rule, the interrogating antennas are oriented so that the slots are parallel to the cross-section of the arm. Body tissues (thickness in [mm], relative permittivity ε_r, conductivity σ in [S/m]): bone (7.5, 20.8, 0.33); muscle (26, 55.1, 0.93); fat (2, 5.5, 0.05); skin (1, 41.5, 0.85).

A. IMDs and interrogating antennas

IMDs are emulated by a (13×8 mm^2) rectangular loop hosting the RFID IC in the middle of the longer side (Fig. 2a). Taking into account the effective permittivity of the human body, the electrical size of the implanted loop is not so small compared with the wavelength. Thus, the current distribution is not uniform on the loop perimeter. Numerical simulations showed that the radiated field in the near region outside the arm is mostly with horizontal polarization (w.r.t. the arrangement in Fig. 2c).

To optimally couple with the field of the loop, the considered interrogating antenna is a double-folded patch (external size: 40×25 mm^2, thickness: 3 mm, internal dielectric proprieties: $\varepsilon_r = 1.55$, $\sigma = 6 \cdot 10^{-4}$ S/m) forming an open-end slot (Fig. 2b) whose electric field must be aligned with the larger size of the loop [26]. For the sake of simulation simplicity, above antennas are considered flat, namely without exactly matching the curvature of the body segment. To make the antenna more conformable, the implementation could exploit textile (FELT) or foam (EPDM) substrates, as already experimented by the authors in [37], [38]. A brief discussion of possible impact of the bending in the multi-element transcutaneous link is given in the Appendix.

Both external and implanted antennas are tuned at 867 MHz. In particular, the implanted transponder is optimized with reference to the IC impedance [42] $Z_{IC} = (12 - j120)\ \Omega$ that will be used in the experimental session. A conservative value of chip sensitivity is $p_{IC} = -10$ dBm that is compatible with state-of-the-art RF-chips enabling the interface with external sensors [43].

The two antenna arrangements are mutually rotated of an angle $\varphi = 22.5°$ (Fig. 2c) and the mutual orientation among antennas (indicated by arrows in Fig. 2) is such to preserve the two-plane symmetry, as well as to optimize the transcutaneous coupling as discussed above. Insertion losses for both the multiplexer (sequential feed) and power splitter (simultaneous feed) are assumed to be $L_S = L_M = 0.7$ dB (1.18).

B. Body Model

The body model is a 35 cm-long multi-layer cylinder having the size of a human arm (cross-section view in Fig. 2c). The phantom includes a bone core, muscle, fat and skin whose dielectric properties in UHF band and thicknesses (caption in Fig. 2c) are derived from [39] and [40]. The layered cylinder is included into 3 mm-thickness external shell of epoxy resin ($\varepsilon_r = 4$, $\sigma = 6 \cdot 10^{-3}$ S/m). This shell can be found in typical prosthetic hand socket where the prosthesis is inserted [26]. Interrogating antennas are hosted on the external surface of the shell and hence they are not in direct touch with the skin. This configuration is beneficial to reduce hot spot in the limb and hence to improve efficiency of the antenna [41]. For the application of the interrogating antennas on different body regions, even when a prosthesis is not involved, they could be partly insulated from the skin through an interfacing (soft) ribbon layer and hence the same model can be applied as well. Sensors are placed in the muscle at 5 mm distance from the internal shell of the cylinder.

C. SAR constraints

Fig. 3 shows the simulated[3] electric field amplitude and the corresponding SAR on the cylinder cross-section for the two arrangements of the feeding arrays. Data are referred to 867 MHz and to a total input power $P_G = 1$ W. In the case of a simultaneous feeding scheme, each antenna will be hence fed by $(0.25/L_S)$ W so that a lower SAR is expected w.r.t. the sequential feeding. It is worth reporting that the mutual impedances between the four interrogating antennas, *i.e.* the off-diagonal elements of the impedance matrix, are 10% up to 20% at most of the self-impedances values. This means that the coupling among the patch antennas is modest due to the high losses of the human body, which enforce an electric decoupling. Consequently, the power delivering of each antenna to the tissues is rather local. Nevertheless, for the sake of accuracy, the coupling have been fully accounted in the simulations.

The distribution of electric fields and SAR when the external antennas are powered, one at a time, and in the case of simultaneous power supply, respectively, are shown in Fig. 3. As expected, the simultaneous array generates a more uniform field distribution on the whole cross-section (Fig. 3a) even if with reduced peaks w.r.t. the sequential array. Moreover, the SAR (Fig. 3b) is less localized in the case of simultaneous array with a maximum value, averaged over 10 g, which is 4.5 times smaller than in the other configuration (5.0 W/kg *vs.* 21.9 W/kg). Therefore, since the exposure regulation [45] requests $SAR_{10g} < 4$ W/kg, it follows by linearity that the power emitted by the generator must be less than $P_G^{max} = \{22.6,\ 29.0\}$ dBm for sequential and simultaneous feed, respectively. Accordingly, by considering the power splitter, each antenna in the simultaneous scheme can be sourced by the same maximum power ($P_{G,m} = (29 - 6 - 0.7) = 22.4$ dBm), similar to that of the sequential scheme ($P_{G,m} = (22.6 - 0.7) = 21.9$ dBm). This is a consequence of the modest coupling among antennas so that their effect is practically independent. On the whole, the simultaneous interrogation permits to use nearly the whole available power (30 dBm) without exceeding the SAR limit with the benefit that all the sensors will be sampled at the same time.

[3]Simulations by CST Microwave Studio 2019, Time Domain solver.

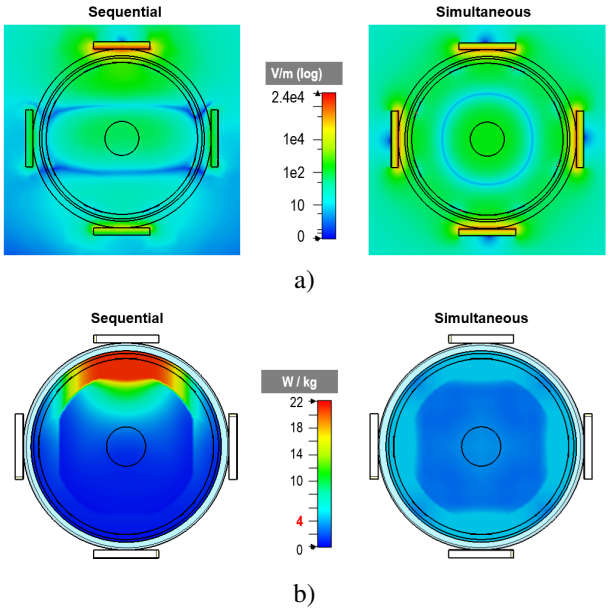

Figure 3. Simulated a) electric field distribution and b) SAR on the cylinder cross-section passing through the center of the interrogating antennas for both the sequential and simultaneous arrays. Results at 867 MHz corresponding to P_G =1 W of available power at the generator.

D. Transducer Gain and Link Margin

Fig. 4 shows the computed *embedded* and *active* transducer power gain for the two array configurations whose antennas are all well tuned to the worldwide UHF RFID band. In case of sequential feeding, IMDs far from the active slot antenna ($S_2 - S_7$ in Fig. 4a) will experience a gain degradation of more than 15 dB w.r.t. the two IMDs (S_1, S_8) just beneath the interrogator R_1. Instead, the gain values are identical for all the IMDs in case of simultaneous feeding. There is however a reduction of 8 dB w.r.t. the best energized IMDs in the sequential feeding, mainly caused by the 1:4 power splitting. Hence, as also found for the field and SAR distributions, the simultaneous feeding provides a much more uniform link gain for all the IMDs, at the expenses of a reduction of the peak values.

The corresponding link margins from (5) are resumed in Tab. I. In case of sequential reading, each reader's antenna is capable to activate two implanted tags with a power margin $M_n = 8.8$ dB. The data rate of the system is hence 2 data samples per read and it implies a minimum power consumption of 12.0 mW for each interrogation, as can be gathered by exploiting eq. (3) and considering the transducer power gain in Fig. 5 at 867 MHz and the chip sensitivity of -10 dBm, as above.

In the simultaneous feeding scheme, instead, all the IMDs will be activated with the same margin $M_n = 7.1$ dB with

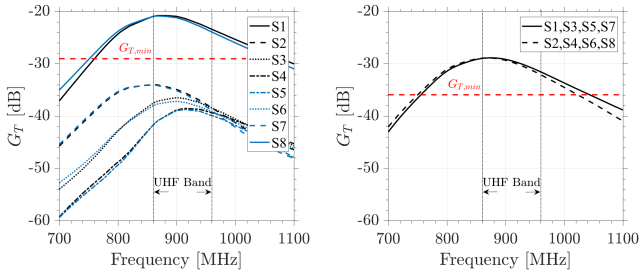

Figure 4. Simulated transducer gains of the reader-sensor ($R_1 - S_n$) transcutaneous links for a) sequential and b) simultaneous feeding schemes.

Table I
CONSTRAINED POWER MARGINS (IN DB) AT 867 MHZ IN CASE OF SEQUENTIALLY AND SIMULTANEOUSLY FED INTERROGATING ARRAYS.

	Sequential				**Simultaneous**
	R_1	R_2	R_3	R_4	
S_1	**8.8**	-4.6	-11.4	-7.6	**7.1**
S_2	-4.4	**8.9**	-8.1	-11.3	**7.1**
S_3	-7.6	**8.9**	-4.6	-11.4	**7.1**
S_4	-11.3	-4.4	**8.8**	-8.1	**7.1**
S_5	-11.3	-7.6	**8.9**	-4.6	**7.1**
S_6	-8.1	-11.2	-4.4	**8.9**	**7.1**
S_7	-4.5	-11.3	-7.5	**8.9**	**7.1**
S_8	**8.8**	-8.1	-11.4	-4.4	**7.1**

respect to the SAR-constrained power $P_G^{max} = 29$ dBm. The expected data rate will be 8 data samples per read. The minimum requested power from the generator is 77.6 mW.

From above numbers, it is clear that the sequential feeding scheme guarantees the interrogation of all the IMDs, but at different times, with the smallest power request and a larger margin. The simultaneous interrogation, providing a four-times data rate, is instead achieved at the expense of extra-power.

E. Tolerance to Misalignment

Finally, the effect of possible angular misalignments between the array and the set of sensors is evaluated with reference to the highest possible displacement of 22.5° occurring when the interrogators are placed just above four sensors (say R_m over $S_{2n-1}, n = 1, ..., 4$). In this case the sensors $\{S_2, S_4, S_6, S_8\}$ will be energized less than sensors $\{S_1, S_3, S_5, S_7\}$. The resulting table of power margins (Tab. II) shows that, in spite of some symmetry lost, all the sensors would be still readable in both the feeding schemes. The smallest power margin reduces of 5 dB (from 8.8 dB down to 3.7 dB) in the case of sequential scheme. The simultaneous architecture is less sensitive to rotations (just a reduction of 2 dB in the link margin). Overall, the system looks resilient with respect to angular misalignments. The vertical misalignment was investigated in [26] and displacements up to 2.5 cm are tolerated.

IV. EXPERIMENTAL EVALUATIONS

The prototypes of interrogating and implanted antennas are shown in Fig. 5a. The experimental mock-up was fabricated through a 3 mm-thick cylinder (external radius 4 cm) made by

Table II
CONSTRAINED POWER MARGINS (IN DB) AT 867 MHZ IN CASE OF ARRAY-IMDS ANGULAR MISALIGNMENT OF 22.5° W.R.T. THE MODEL IN FIG. 2C.

	Sequential				**Simultaneous**
	R_1	R_2	R_3	R_4	
S_1	**12.6**	-11.6	-6.3	-12.5	**7.4**
S_2	-0.03	**3.8**	-13.9	-6.9	**5.3**
S_3	-12.5	**12.6**	-11.6	-6.3	**7.4**
S_4	-6.9	-0.1	**3.7**	-13.9	**5.3**
S_5	-6.3	-12.5	**12.5**	-11.6	**7.4**
S_6	-14.0	-6.8	-0.2	**3.8**	**5.3**
S_7	-11.6	-6.3	-12.5	**12.5**	**7.4**
S_8	**3.8**	-13.9	-6.9	-0.1	**5.3**

epoxy resin (Fig. 5b.1) that emulates the socket of a hand prosthesis. The external microstrip slots were fixed on the cylinder by insulating tape. The IMDs loops hosts the Impinj Monza R6-P IC [42] with auto-tune disabled. The sensitivity of the microchip is $p_{IC} = -20$ dBm but the results given next will be scaled as in [26] to the reference value $p_{IC} = -10$ dBm for typical sensor-oriented ICs. Loops were attached over an ultra-thin substrate of PET forming a cylindrical surface of 3.4 cm radius (Fig. 5b.2). The space between the concentric external and internal cylinders was filled by minced meat [26], emulating both the skin and the fat layers (Fig. 5b.3). The remaining part of the cylinder was then also filled by the minced meat emulating the muscle (Fig. 5b.4). To implement the sequential feeding case, an AdvanSplitter-4 by Keonn [46] was interconnected between the generator and the antennas (Fig. 5c).

The embedded reflection coefficients Γ_m of each external reader's antenna in Fig. 5a was preliminarily measured by a Vector Network Analyzer, in the presence of all the other slot antennas in open-circuit termination, and of all the implanted loops, each connected to its RFID IC. Results are shown in Fig. 6 in comparison with the simulation. There is some variability among the four antennas. They have been fabricated manually with adhesive copper and an hand cutter. Thus, a fabrication uncertainty of at least 0.5 mm is expected in any size of the device. Furthermore, the resonance frequency is rather sensitive to the width of the vertical strips, and they were also trimmed by hand. Not least, even though the authors made their best to guarantee a homogeneous filling of the minced meat to avoid air inclusion, it is possible that the antennas see not identical local permittivity. Overall, the maximum frequency shift among the measured resonance frequencies is roughly 50 MHz around 900 MHz that means a maximum error of 6 %. Nevertheless, all the four antennas exhibit a reflection coefficient smaller than -15 dB in the RFID-UHF band. The achieved performance are hence suitable to demonstrate the idea. A more repeatable, and still tunable antenna could be fabricated through etching and removable vias to emulate the effect of the vertical tuning strips.

A. Power margin measurements

The measurements of both the sequential and the simultaneous feeding schemes were performed by using the Voyantic

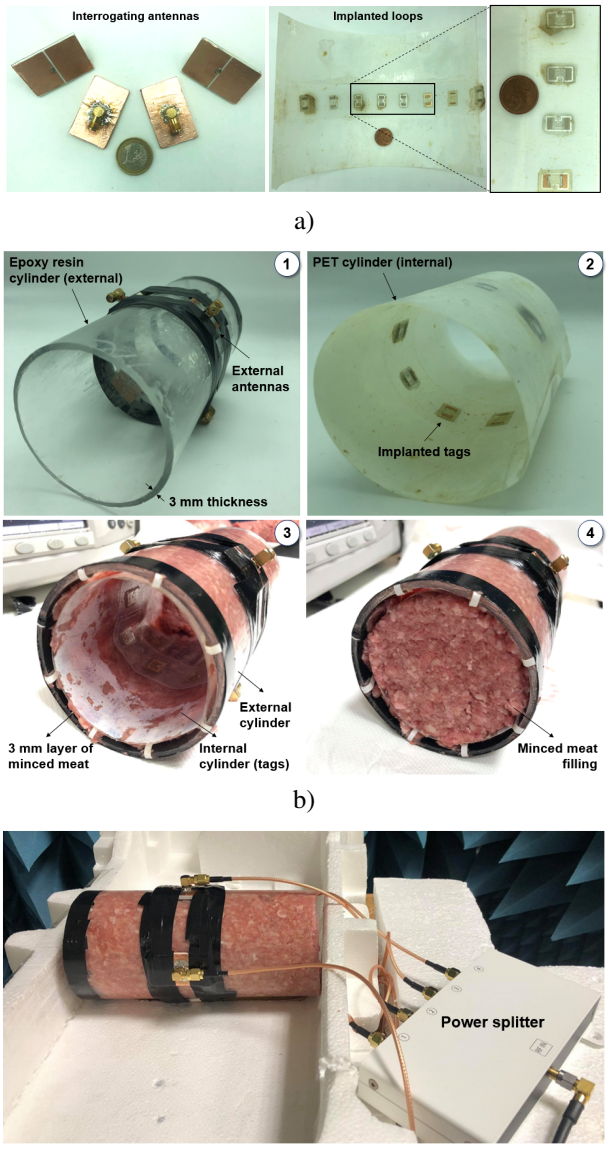

Figure 5. a) Prototypes of the microstrip slots and of the implantable loops. b) Experimental mock-up: the epoxy resin pipe (1), emulating the prosthetic socket, was used as a support for the external array and the PET cylinder for the accurate positioning of implanted sensors (2); a first layer of 3 mm of minced meat was inserted between epoxy resin pipe and PET cylinder (3), emulating both fat and skin tissues, and finally the remaining part was filled with minced meat (4). c) In the simultaneous feeding scheme the interrogating slot are connected to a 1:4 power splitter.

TagFormance Station. The system returns the minimum activation power of each readable IMD and then the transducer power gain is derived from (3). By accounting the SAR constraints (Section III-C) and the chip sensitivity $p_{IC} = -10$ dBm, the power margin was then calculated as in (5). The results are shown in Fig. 7 for $\{R_1, R_2, R_3, R_4\}$ individually powered (Fig. 7a-b-c-d, respectively) and for the simultaneous feeding of the circular array (Fig. 7e). Concerning the sequential feeding, each interrogating antenna communicates with the sensors implanted below with a positive margin $M > 0$ dB. The differences in the communication performance among

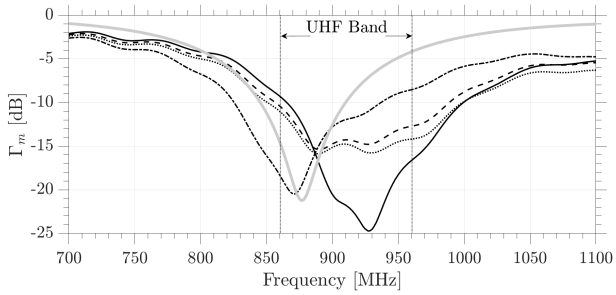

Figure 6. Measured reflection coefficients of the interrogating antennas and comparison with simulations.

some IMDs placed in symmetric positions are probably due to manufacturing imperfections of all the components of the system, including the mockup. Finally, the margin for the simultaneous feeding scheme is shown in Fig. 7e. All the IMDs have a positive margin and also in this case results compare satisfactorily with the model.

V. Conclusions

The potentiality of a circular array of interrogating antennas has been exploited, both numerically and experimentally, to establish a robust RFID link with implanted devices placed into a cylindrical body region. By accounting for the SAR constraints on the maximum power the reader is allowed to emit, the sequential scheme is the least power-hungry, also guaranteeing the largest power margin. Even in extreme conditions (the whole margin used), the required power to energize up to eight devices hosting the state-of-the-art sensor-oriented ICs, is less than 23 dBm. This value is well compatible with portable small readers. Due to the limited sampling rate (two samples per reading), sequentially fed arrays could be suitable for the monitoring of slow-varying physiologic parameters, such as the deformation. Instead, when faster events have to be sampled, such as bio-electric signals from muscles, the simultaneous feeding scheme must be used. It permits a higher data rate, up to 8 data samples per reading, but at the price of a not negligible increase of the feeding power. Anyway, miniaturized readers with an output power of 25 dBm at least, could be applied with still a residual margin of 3 dB. The array is moreover rather tolerant to angular misalignment with respect to the arrangement of the implanted sensors with great benefit to practical implementation when antennas must be integrated within a prosthetic socket. Instead, in case of direct application onto other parts of the body without any fixed prosthesis, provided that the interrogating antennas are mutually linked through a dielectric ribbon, their optimal position can be found based on a real-time measurement of the Received Signal Strength Indicator (RSSI) returned by the sensors. The ribbon is moved around until the position with the best link is identified. This procedure could be also supervised by an ad-hoc software supporting the operator to set-up the optimal arrangement.

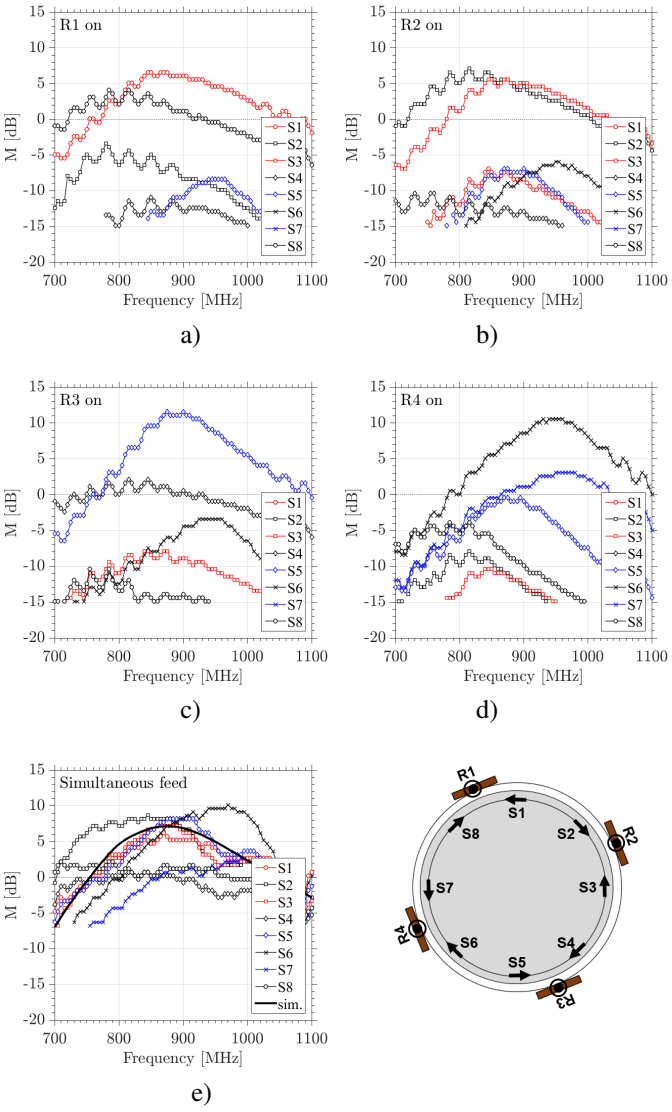

Figure 7. Measured power margins in the case of sequential feed of reader's antenna a) R_1, b) R_2, c) R_3, d) R_4 and e) when all slot antennas are simultaneously powered.

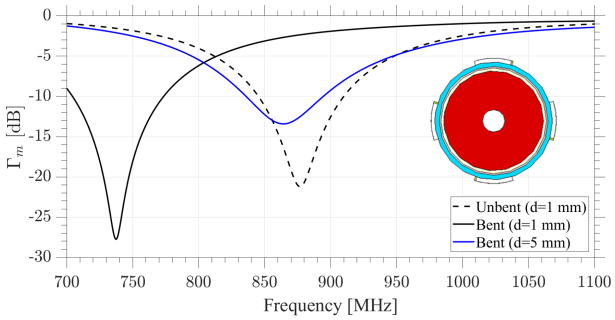

Figure 8. Simulated reflection coefficient of the interrogating antennas when perfectly wrapped onto the curved surface of the cylinder. Comparison with the original un-bent configuration and with a modified version where the width d of tuning shorting strips is enlarged to retune the resonance frequency at 867 MHz.

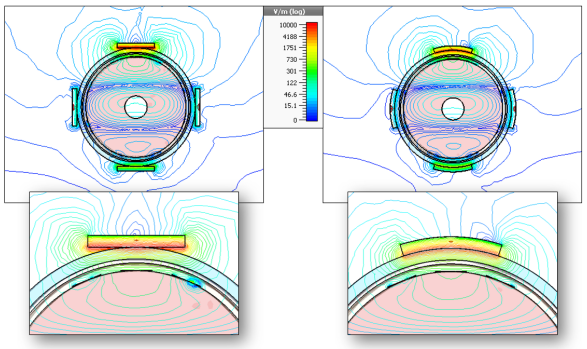

Figure 9. Distribution of electric field at 867 MHz is reported for each optimized configuration.

APPENDIX: EFFECT OF BENDING OF THE INTERROGATING ANTENNAS

In real applications, the double patch antennas could be more comfortably bent to match the curvature of the body. The inset in Fig. 8 shows the cross-section of the cylinder with a perfectly wrapped antenna over it, with a curvature angle of 37°. The expected impact are on the resonant frequency and on the distribution of the internal field.

Frequency shift

Numerical simulation revealed that the bending produces a not negligible downward-shift of the resonance frequency of more than 100 MHz. This change can be compensated by acting on the tuning short circuit, moving from $d = 1$ mm to $d = 5$ mm (Fig. 8).

Field distribution

Field distribution inside the cylinder is mostly due to the slot that is partially affected by bending. However, there is no relevant modification of the electric field w.r.t. the case of the flat antenna (Fig. 9). Hence, the coupling with the sensors will be unchanged. Indeed, the computation of the power margin for both sequential and simultaneous feeds shows similar (and even better in the sequential case) power values (9.2 - 9.5 dB and 6.9 - 7.1 dB, respectively) that those of the flat case (8.8 dB and 7.1 dB, respectively).

Overall, the bending mostly disturbs the detuning of the interrogation antennas and hence, for real applications, the on-body antenna must be fabricated with a rigid substrate having a moderate curvature (for instance by glueing a flexible antenna as before over a pre-formed curved holder) so that the limb shape is at least partly matched as already done in hyperthermia applicators.

ACKNOWLEDGMENTS

This work was supported by IIT (Istituto Italiano di Tecnologia) and INAIL-CP (Istituto Nazionale Assicurazione Infortuni sul Lavoro—Centro Protesi), under contract PPR AS 1/1, Task 1.5.

REFERENCES

[1] A. Kiourti, and K. S. Nikita, "A Review of In-Body Biotelemetry Devices: Implantables, Ingestibles, and Injectables," *IEEE Transactions in Biomedical Engineering*, vol. 64, no. 7, pp. 1422-1430, July 2017.

[2] N. A. Malik, P. Sant, T. Ajmal, and M. Ur-Rehman, "Implantable Antennas for Bio-medical Applications," *IEEE Journal of Electromagnetics, RF and Microwaves in Medicine and Biology*, Oct. 2020, early access.

[3] S. Shim, K. Seo, and S. J. Kim, "A preliminary implementation of an active intraocular prosthesis as a new image acquisition device for a cortical visual prosthesis," *Journal of Artificial Organs*, vol. 23, pp. 262-269, Apr. 2020.

[4] N. Even-Chen, D. G. Muratore, S. D. Stavisky, L. R. Hochberg, J. M. Henderson, B. Murmann, and K. V. Shenoy, "Power-saving design opportunities for wireless intracortical brain–computer interfaces," *Nature Biomedical Engineering*, vol. 4, pp. 984-996, Aug. 2020.

[5] F. Cavrini, L. Bianchi , L. R. Quitadamo, and G. Saggio, "A fuzzy integral ensemble method in visual P300 brain-computer interface," *Computational intelligence and neuroscience*, Jan. 2016.

[6] H. Zhang, et al., "Wireless, battery-free optoelectronic systems as subdermal implants for local tissue oximetry," *Science Advances*, vol. 5, no. 3, Mar. 2019.

[7] R. S. Hassan, J. Lee, and S. Kim, "A Minimally Invasive Implantable Sensor for Continuous Wireless Glucose Monitoring Based on a Passive Resonator," *IEEE Antennas and Wireless Propagation Letters*, vol. 19, no. 1, pp. 124-128, Jan. 2020.

[8] G. Saggio, "Are Sensors and Data Processing Paving the Way to Completely Non-invasive and Not-painful Medical Tests for Widespread Screening and Diagnosis Purposes?," *13th International Joint Conference on Biomedical Engineering Systems and Technologies (BIOSTEC 2020)*, Valletta, Malta, Feb. 24-26, 2020.

[9] F. Fries, and S. Ghoreishizadeh, "Design Methodology of a Wireless pH Measuring Device for Orthopaedic Implants," 27th IEEE International Conference on Electronics, Circuits and Systems (ICECS), Glasgow, UK, 23-25 Nov. 2020.

[10] K. S. Mitchell, W. Anderson, T. Shay, J. Huang, M. Luciano, J. I. Suarez, P. Manson, H. Brem, and C. R. Gordon, "First-In-Human Experience With Integration of Wireless Intracranial Pressure Monitoring Device Within a Customized Cranial Implant," *Operative Neurosurgery*, vol. 19, no. 3, pp. 341-350, Sept. 2020.

[11] R. Lodato, V. Lopresto, R. Pinto, and G. Marrocco, "Numerical and experimental characterization of through-the-body UHF-RFID links for passive tags implanted into human limbs," *IEEE Transactions on Antennas and Propagation*, vol. 62, no. 10, pp. 5298–5306, Oct. 2014.

[12] R. Bashirullah, "Wireless Implants," *IEEE Microwave Magazine*, vol. 11, no. 7, pp. S14-S23, Dec. 2010

[13] A. Kiourti, and K. S. Nikita, "Implantable Antennas: A Tutorial on Design, Fabrication, and In VitroVIn Vivo Testing," *IEEE Microwave Magazine*, vol. 15, no. 4, pp. 77-91, June 2014.

[14] A. Sani, M. Rajab, R. Foster, and Y. Hao, "Antennas and Propagation of Implanted RFIDs for Pervasive Healthcare Applications," *Proceedings of the IEEE*, vol. 98, no. 9, pp. 1648-1655, Sept. 2010.

[15] C. Occhiuzzi, G. Contri, and G. Marrocco, "Design of implanted RFID tags for passive sensing of human body: The STENTag," *IEEE Transactions on Antennas and Propagation*, vol. 60, no. 7, pp. 3146–3154, July 2012.

[16] S. Amendola, E. Moradi, K. Koski, T. Björninen, L. Sydänheimo, L. Ukkonen, J. M. Rabaey, Y.Rahmat-Samii, "Design and Optimization of mm-Size Implantable and Wearable On-Body Antennas for Biomedical Systems," *8th European Conference on Antennas and Propagation (EuCAP 2014)*, The Hague, Netherlands, 6-11 Apr. 2014.

[17] D. Dobkin, *The RF in RFID: UHF RFID in Practice*, Elsevier Science, Dec. 2012.

[18] A. Kiourti, "RFID Antennas for Body-Area Applications: From Wearables to Implants," *IEEE Antennas and Propagation Magazine*, vol. 60, no. 5, pp. 14-25, Oct. 2018.

[19] C. Miozzi, S. Guido, G. Saggio, E. Gruppioni, and G. Marrocco, "Feasibility of an RFID-based transcutaneous wireless communication for the control of upper-limb myoelectric prosthesis," *12th European Conference on Antennas and Propagation (EuCAP 2018)*, London, UK, 9-13 April 2018.

[20] C. Miozzi, V. Errico, G. Saggio, E. Gruppioni and G. Marrocco, "UHF RFID-Based EMG for Prosthetic Control: preliminary results," *2019 IEEE International Conference on RFID Technology and Applications (RFID-TA)*, Pisa, Italy, 25-27 Sept. 2019.

[21] G. Li, Y. Li, L. Yu, and Y. Geng, "Conditioning and Sampling Issues of EMG Signals in Motion Recognition of Multifunctionl Myoelectric Prostheses," *Annals of Biomedical Engineering*, vol. 39, no. 6, pp. 1779-1787, 2011.

[22] D. J. Yeager, J. Holleman, R. Prasad, J. R. Smith, and B. P. Otis, "NeuralWISP: A Wirelessly Powered Neural Interface With 1-m Rang," *Trans. on Biomedical Circuits and Systems*, vol. 3, no. 6, 2009.

[23] R. Horne, J. Batchelor, P. Taylor, E. Balaban and A. Casson, "Ultra-Low Power on Skin ECG using RFID Communication," *IEEE International Conference on Flexible and Printable Sensors and Systems (FLEPS)*, Manchester, UK, 16-19 Aug. 2020.

[24] A. Krasoulis, S. Vijayakumar, K. Nazarpour, "Multi-Grip Classification-Based Prosthesis Control With Two EMG-IMU Sensors," *IEEE Trans. Neural Syst. Rehabil. Eng.*, vol. 28, no. 2, pp. 508-518, 2020.

[25] M. W. A. Khan, L. Sydänheimo, L. Ukkonen, and T. Björninen, "Inductively Powered Pressure Sensing System Integrating a Far-Field Data Transmitter for Monitoring of Intracranial Pressure," *IEEE Sensors Journal*, vol. 17, no. 7, pp. 2191-2197, Apr. 2017.

[26] C. Miozzi, G. Saggio, E. Gruppioni, and G. Marrocco, "Constrained Safety-Integrity Performance of Through-the-Arms UHF-RFID Transcutaneous Wireless Communication for the Control of Prostheses," *IEEE Journal of Radio Frequency Identification*, vol. 3, no. 4, pp. 236-244, Dec. 2019.

[27] L. Zhang, Y. Zhu, T. Mo, J. Hou, and H. Hu, "Design of 3D Positioning Algorithm Based on RFID Receiver Array for In Vivo Micro-Robot," *8th IEEE International Conference on Dependable, Autonomic and Secure Computing*, Chengdu, China, 12-14 Dec. 2009.

[28] A. R. Nafchi, S. Ting Goh, and S. A. Reza Zekavat, "Circular Arrays and Inertial Measurement Unit for DOA/TOA/TDOA-Based Endoscopy Capsule Localization: Performance and Complexity Investigation," *IEEE Sensors Journal*, vol. 14, no. 11, pp. 3791-3799, Nov. 2014.

[29] M. Pourhomayoun, Z. Jin, and M. L. Fowler, "Accurate localization of in-body medical implants based on spatial sparsity," *IEEE Transactions on Bio-medical Engineering*, vol. 61, no. 2, pp. 590-597, Feb. 2014.

[30] F. Bianchi, A. Masaracchia, E. S. Barjuei, A. Menciassi, A. Arezzo, A. Koulaouzidis, D. Stoyanov, P. Dario, and G. Ciuti, "Localization strategies for robotic endoscopic capsules: a review," *Expert Review of Medical Devices*, vol. 16, no. 5, pp. 381-403, May 2019.

[31] F. Bardati, A. Borrani, A. Gerardino, and G. A. Lovisolo, "SAR Optimization in a Phased Array Radiofrequency Hyperthermia System," *IEEE Transactions on Biomedical Engineering*, vol. 42, no. 12, pp. 1201-1207, Dec. 1995.

[32] F. Bardati, and P. Tognolatti, "Hyperthermia phased arrays pre-treatment evaluation," *International Journal of Hyperthermia*, vol. 32, no. 8, pp. 911-922, Oct. 2016.

[33] M. M. Paulides, J. F. Bakker, N. Chavannes, and G. C. Van Rhoon, "A Patch Antenna Design for Application in a Phased-Array Head and Neck Hyperthermia Applicator," *IEEE Transactions on Biomedical Engineering*, vol. 54, no. 11, pp. 2057-2063, Nov. 2007.

[34] K. Agarwal, R. Jegadeesan, Y. Guo, and N. V. Thakor, "Wireless Power Transfer Strategies for Implantable Bioelectronics," *IEEE Reviews in Biomedical Engineering*, vol. 10, pp. 136-161, Mar. 2017.

[35] Keonn AdvanMux-4, RFID UHF multiplexer (Accessed June 21, 2021). [Online]. Available: https://keonn.com/wp-content/uploads/Keonn-AdvanMux-4-Data-sheet.pdf.

[36] CAEN RFID qIDmini, RFID handheld reader (Accessed June 21, 2021). [Online]. Available: https://www.caenrfid.com/en/products/r1170i-qidmini/.

[37] S. Manzari, C, Occhiuzzi, G. Marrocco, "Feasibility of Body-centric Systems by Using passive textile RFID tags," *IEEE Antennas and Propagat. Magaz.*, vol. 54, no. 9, pp. 2851-2858, 2012.

[38] S. Manzari, S. Pettinari, G. Marrocco, "Miniaturized wearable UHF-RFID tag with tuning capability," *Electronics Letters*, vol. 48, no. 21, pp. 1325–1326, 2012.

[39] *Dielectric Properties of Human Body* (Accessed Oct. 19, 2020). [Online]. Available: http://niremf.ifac.cnr.it/tissprop/.

[40] D. Marques, M. Egels, and P. Pannier, "Broadband UHF RFID Tag Antenna for Bio-Monitoring," *Progress In Electromagnetics Research B*, vol. 67, no. 1, pp. 31-44, Jan. 2016.

[41] S. Amendola, G. Marrocco, "Optimal Performance of Epidermal Antennas for UHF Radiofrequency Identification and Sensing," *IEEE Trans. on Antennas and Propagat.*, vol. 65, no. 2, pp. 473–481, Feb. 2017.

[42] Impinj Monza R6-P IC (Accessed Oct. 19, 2020). [Online]. Available: https://support.impinj.com/hc/en-us/articles/204793258-Monza-R6-P-Product-Brief-Datasheet.

[43] Asygn AS3212 IC (Accessed Feb. 27, 2021). [Online]. Available: https://asygn.com/as321x/#as3211.
[44] S. J. Orfanidis, *Electromagnetic Waves and Antennas*, 2016 (Accessed Oct. 19, 2020). [Online]. Available: https://www.ece.rutgers.edu/~orfanidi/ewa/.
[45] *Limitation of Exposure of the General Public to Electromagnetic Fields*, European Council Recommendation 1999/519/EC, 12 July 1999 [Online]. Available: http://ec.europa.eu/enterprise/electr_equipment/lv/rec519.pdf, (0 Hz to 300 GHz, Official Journal, L199, 30.7.1999., pp.59).
[46] Keonn AdvanSplitter-4, RFID UHF power splitter (Accessed Oct. 19, 2020). [Online]. Available: https://keonn.com/wp-content/uploads/2020/01/Keonn-AdvanSplitter-4-Data-sheet-2.pdf.